NASA Technical Memorandum 100416

A Comparison of Experimental and Calculated Thin-Shell Leading-Edge Buckling Due to Thermal Stress

Jerald M. Jenkins

July 1988

National Aeronautics and
Space Administration

NASA Technical Memorandum 100416

A Comparison of Experimental and Calculated Thin-Shell Leading-Edge Buckling Due to Thermal Stress

Jerald M. Jenkins
Ames Research Center, Dryden Flight Research Facility, Edwards, California

1988

NASA
National Aeronautics and
Space Administration
Ames Research Center
Dryden Flight Research Facility
Edwards, California 93523-5000

SUMMARY

High-temperature thin-shell leading-edge buckling test data are analyzed using NASA structural analysis (NASTRAN) as a finite element tool for predicting thermal buckling characteristics. Buckling points are predicted for several combinations of edge boundary conditions. The problem of relating the appropriate plate area to the edge stress distribution and the stress gradient is addressed in terms of analysis assumptions. Local plasticity was found to occur on the specimen analyzed, and this tended to simplify the basic problem since it effectively equalized the stress gradient from loaded edge to loaded edge. The initial loading was found to be difficult to select for the buckling analysis because of the transient nature of thermal stress. Multiple initial model loadings are likely required for complicated thermal stress time histories before a pertinent finite element buckling analysis can be achieved. The basic mode shapes determined from experimentation were correctly identified from computations.

INTRODUCTION

The prediction of the buckling point of flat plates subjected to thermal stresses is a complicated problem of emerging significance. The contemporary problem of boundary condition definition is complicated in the elevated temperature situation by the presence of two-dimensional nonlinear variations in thermal stress. Mathematical approaches to such problems are formidable; however, finite element computer programs provide a means for a solution.

The purpose of this report is to analyze previous buckling test data (Jenkins and Sefic, 1966) using NASA structural analysis (NASTRAN) (NASA-COSMIC, 1983) as the means to predict the buckling point. Test data were acquired defining the buckling points of thin-shell leading-edge specimens of varying dimensions. Buckling boundaries were established empirically because at the time of the test neither analysis tools nor strain sensors were available to define the stress pattern at elevated temperatures. The measured temperature data are used to compute thermal stresses, and the resulting thermal stress distribution is used as the loading from which eigenvalues are computed for the first three buckling mode shapes. The computed point at which buckling is expected to occur is compared with the actual point at which buckling did occur.

NOMENCLATURE

A	numerical coefficient
a	plate length, in.
b	plate width, in.
cl	center line
D	flexural rigidity of plate $D = Eh^3/12(1-\nu^2)$
E	modulus of elasticity, lb/in.^{2}
$f(t)$	mathematical description of thermal stress as a function of time, lb/in.^{2}
h	plate thickness, in.
k	numerical coefficient
m, n	integers, numerical factors
N_x, N_y, N_{xy}	normal and shearing forces per unit distance in the middle surface of plate
T	temperature, F°

t	time, sec
w	warping displacement in the z direction, in.
x, y, z	rectangular coordinates, in.
η	numerical coefficient
λ	eigenvalue, numerical factor
ν	Poisson's ratio
σ_{cr}	critical buckling stress, lb/in.^{2}
σ_T	thermal stress, lb/in.^{2}
σ_Y	yield stress, lb/in.^{2}

EXPERIMENTAL DATA

One of the 51 flanged, thin-shell leading-edge specimens tested by Jenkins and Sefic (1966) has been selected for detailed examination. The basic geometry of the specimen is shown in figure 1(a) where specific dimensions are identified. The material of the specimen is the nickel-based alloy Inconel X-750. The length of the specimen was 16.0 in. and the taper angle was 15°. A channel of 0.080-in. material with a 1.0-in. flange was spot-welded to the specimen as shown in figure 1(a). The specimens were given a full heat treatment (Syracuse University, 1982). Prior to experimentation, each of the specimens was instrumented with externally mounted chromel-alumel thermocouples (fig. 1(b)). Appropriate structural restraint was provided by a 4I7.7 steel beam by milling off the outside 0.4 in. of the top of the flanges as shown in figure 1(c). The thermocouples were located at the stagnation line, at 0.38, 1.50, and 2.50 in. below the stagnation line.

A sketch of the assembled test is shown in figure 2. A bank of radiant heat lamps was arranged about the upper 1.00 in. of the specimen. External heat transfer was allowed only on the radial portion of the specimen. The remainder of the specimen was protected from radiant heat by sheets of high-temperature insulation. The specimen was attached to the beam by inserting bearing plates inside the specimen and passing symmetrically positioned stainless steel bolts through the bearing plate, through the web of the channel, and finally through the flange of the beam.

A control thermocouple was positioned on the stagnation line of the cylindrical part of the leading-edge specimen 8 in. from each end. The heating of the specimen was controlled with this thermocouple. The temperature along the stagnation line was programmed to rise from room temperature at a rate of 50°F per sec to 1700°F. The temperature was held at this level for 10 sec. Four additional thermocouples were installed on the specimen to monitor chord temperature gradients. The locations of the thermocouples are shown on figure 1(b). The experiment was conducted by heating the specimen according to the temperature-time history of figure 3. Temperatures were recorded continuously, and observers noted the occurrence of buckling. Details not included in this report may be found in Jenkins and Sefic (1966).

BUCKLING MODES

The basic information obtained from the experimental test of the specimen shown in figure 1(a) included (1) the manner in which the specimen buckled, (2) the stagnation point temperature at the time of buckling, and (3) the temperature distribution at the time of buckling. Two modes of unstable behavior were observed as shown in figure 4. Mode A occurred in the central region of the specimen flanges. This mode of buckling was either a single or multiple wave pattern similar to the buckling of a plate compressed

in one direction with unequal restraint on the edges parallel to the compression. The specific dimensions of the wave patterns were not recorded. Mode B buckling also occurred in the flanges of the specimen. This mode of buckling was a single-wave pattern similar to that in a compressed thin column. The two types of buckling failures occurred in the flat sections of the specimens, reflecting the greater stability of curved or shell type areas relative to the flat or plate type areas. Therefore, the analysis was approached as a plate problem.

ANALYTICAL CONSIDERATIONS

The basic geometrical considerations for formulating a plate buckling problem are the width b, length a, and thickness h (fig. 5). The pertinent forces are the normal forces N_x and N_y and the shear forces $N_{xy} = N_{yx}$. The other pertinent variables are the stiffness of the plate and the boundary conditions at the edges of the plate.

Plate buckling is approached analytically by examining the energy of bending and the work done by the edge forces for all mode shapes. The plate is stable if the energy of bending is greater than the work done by the edge forces for all mode shapes. The plate is unstable if the energy of bending is less than the work done by the edge forces for one or more mode shapes.

The basic differential equation (Timoshenko and Gere, 1961) for the buckled plate is

$$\frac{\partial^4 w}{\partial x^4} + 2\frac{\partial^4 w}{\partial x^2 \partial y^2} + \frac{\partial^4 w}{\partial^4 y} = \frac{1}{D}\left(N_x \frac{\partial^2 w}{\partial x^2} + N_y \frac{\partial^2 w}{\partial y^2} + 2N_{xy}\frac{\partial^2 w}{\partial y \partial x}\right) \tag{1}$$

The most commonly used solution of equation (1) is

$$w = \sum_{m=1}^{\infty} \sum_{n=1}^{\infty} A_{mn} \sin \frac{m\Pi x}{a} \sin \frac{n\Pi y}{b} \tag{2}$$

The basic boundary conditions reflecting edge conditions of zero deflection, zero rotation, zero bending, and zero shear are, respectively,

$$w = 0 \tag{3}$$

$$\frac{\partial w}{\partial y} = 0 \quad , \quad \frac{\partial w}{\partial x} = 0 \tag{4}$$

$$\frac{\partial^2 w}{\partial y^2} + \nu \frac{\partial^2 w}{\partial x^2} = 0 \quad , \quad \frac{\partial^2 w}{\partial x^2} + \nu \frac{\partial^2 w}{\partial y^2} = 0 \tag{5}$$

$$\frac{\partial^3 w}{\partial y^3} + (2-\nu)\frac{\partial^3 w}{\partial x^2 \partial y} = 0 \quad , \quad \frac{\partial^3 w}{\partial x^3} + (2-\nu)\frac{\partial^3 w}{\partial y^2 \partial x} = 0 \tag{6}$$

The classical approach to plate buckling has been to solve equation (1) with the solution of equation (2) for sets of the boundary conditions in equations (3) through (6). This has provided a wide variety of analytically solved problems (Gerard and Becker, 1957). When thermal stresses are the source of the load, the problem changes in nature in three ways, as follows: (1) various parts of the plate are at different temperatures, hence, there is a nonuniform stiffness; (2) the edge loadings are nonlinear; and (3) the stress field may vary in two directions, thus complicating the definition of the edge loads. These factors render an analytical solution nearly impossible. As will be shown later in this report, these factors considerably complicate a solution even with finite element computational capability.

STRESS MODEL

A NASTRAN (NASA-COSMIC, 1983) stress model of a symmetrical one-quarter of the test specimen was developed as shown in figure 6(a). An end view of the model is shown in figure 6(b). The model was developed using plate elements for the specimen and a bar element for the restraining beam. The bar element was developed with a moment of inertia value of half of the beam. Temperatures recorded during the test (Jenkins and Sefic, 1966) were smeared to the grid points, and thermal stresses were calculated. Isostresses for axial normal thermal stress and lateral normal thermal stress are shown in figures 7(a) and 7(b), respectively. These stress distributions will be used to define edge loadings for the NASTRAN buckling model.

BUCKLING MODEL

The area of the test specimen modeled for buckling analysis (NASTRAN) is shown in figure 8. The center half of the flat region was selected for modeling so that sufficient elements were available to define the mode shapes. The loading (fig. 8) that was applied to the model is obtained from the thermal stress model (figs. 6 and 7) for temperatures occurring at 30 sec (fig. 4). This is the load distribution used as the baseline loading for the NASTRAN buckling runs (solution 5,0). The eigenvalues provide factors by which the baseline loading may be multiplied to obtain the edge loading at a buckling condition. The inverse power method (symmetric matrix operations) was used as the eigenvalue extraction approach.

RESULTS AND DISCUSSION

Mode A Analysis

Since the boundary condition at the edges is a primary uncertainty in most cases, a matrix of different boundary condition combinations was selected to determine the extent of the variation in calculated buckling point (eigenvalue). Since the bottom edge of the area to be analyzed was spot welded to a heavier doubler, it was concluded that this edge should be clamped. This leaves the upper edge where the circular part of the specimen begins and the two end edges as boundary conditions to be varied. This leaves four combinations of boundary conditions to be examined, as follows: (1) upper edge simply supported with the ends simply supported, (2) upper edge simply supported with the ends clamped, (3) upper edge clamped with ends simply supported, and (4) upper edge clamped with ends clamped.

These four boundary conditions were used with the baseline loading to obtain NASTRAN runs defining the eigenvalues for the first three mode shapes (fig. 9). The mode shapes of the buckled plate are shown for the first three modes for the four combinations of boundary conditions discussed in the previous paragraph.

Thermal stress is induced by the temperature field of the structure. The temperatures within a structure are rarely steady state, meaning that transient temperatures result in transient thermal stresses. If the thermal stress is inherently transient, then the thermal stress distribution at one instant is different from the previous instant. This presents a problem since an edge-loading shape must be derived from the edge thermal stresses to conduct the buckling analysis. This forces the analyst to select one of many possible thermally induced edge load distributions as the basis for eigenvalue extraction. Thermal buckling becomes a very complicated problem if the temperature field inducing thermal stress is highly transient. It is quite possible that the analyst may have to extract eigenvalues for several edge load distributions. In most cases, the pertinent thermal stress distribution will correspond to the largest temperature gradient. This approach was taken for the leading edge in this paper. The maximum temperature gradient occurs at

time = 30 sec (fig. 4). The thermal stress distribution at this time was chosen as the baseline loading to be distributed to the appropriate grid points. Therefore, if the general expression for transient thermal stress is

$$\sigma_T = f(t) \tag{7}$$

then the baseline distribution of thermally induced edge load would be

$$\sigma_T = f(30.0) \tag{8}$$

The thermal stress at failure which the NASTRAN program computes is a multiplying factor (eigenvalue) of the stress distribution, or

$$\sigma_T = \lambda f(30.0) \tag{9}$$

Since experimental knowledge is available concerning when the specimen buckled, then the distribution of thermal stress at the time of buckling can be computed by inputting the temperature distribution at the time of failure (in this case time = 20.5 sec) into the stress model. This thermal stress distribution is designated

$$\sigma_T = f(20.5) \tag{10}$$

The thermal stress distribution relating to equations (8), (9), and (10) are presented in figure 10. The baseline thermal stress, equation (8), is represented by the solid line. The thermal stress distribution at the time of actual buckling corresponds to equation (10). Since there is an eigenvalue for each of the first three mode shapes and there are four sets of boundary conditions, there are twelve results for equation (9). There are four values for equation (9) if only the eigenvalues for the first modes are used. The range of these values is shown as the cross-hatched area in figure 10.

The results of figure 10 are also compared to the exact solution for the buckling of a simply supported rectangular plate under combined bending and compression as found in Timoshenko and Gere (1961). The expression for the critical buckling stress is

$$\sigma_{cr} = k\frac{\pi^2[Eh^3/12(1-\nu^2)]}{b^2h} \tag{11}$$

Estimates of the numerical factor k and the elastic modulus E were required. The value of k was extrapolated to be 23.1 and the value of E was estimated to be 24.0×10^6 lb/in.^{2} to account for temperature degradation. This solution is presented as the solid line in figure 10. The critical buckling stress based on this approach appears to be less than the other results. Since all the edges for this computed value are presumed to be simply supported, the result is not unexpected.

There are several observations that can be made from the results to this point. The modal shapes are quite complex. The number of half-waves that the model exhibits implies that a smaller area could satisfactorily suffice as an appropriate model. The range of eigenvalues for the various boundary conditions is closely packed. This is encouraging from an analyst's viewpoint because the definition of the boundary conditions is a complex issue. A skin panel attached to spars or ribs at all four edges is best described as having a clamped restraint at the edge boundaries. Since some axial rotation of the spars and ribs is probable, then the boundary condition lies somewhere between clamped and simply supported. The infinitely long compressed plate of Gerard and Becker (1957) shows a 70 to 80 percent change in buckling strength (eigenvalue) when the boundary conditions are changed from simply supported to clamped. The eigenvalues calculated for the thermal stress problem in this paper show no more than 10 percent changes when boundary conditions are changed from simply supported to clamped. This discrepancy is attributed to the fact that the plate edge loading in Gerard and Becker (1957) is uniform while the edge loading

due to thermal stress is highly nonuniform. The temperature-induced nonuniform stiffness of the plate elements may also contribute to this discrepancy. The nature of the edge loading is a factor the designer must consider in evaluating the significance of the boundary conditions.

The results presented in figure 10 strongly suggest that the buckling stress can be accurately predicted for this problem. In this case where the leading-edge temperature is consistently increasing, the shape of the thermal stress function $f(t)$ is similar for the range of times. The case where the heat input is increasing and decreasing would be more difficult to analyze since the baseline thermal stress distribution would be a widely varying function. Where the function $f(t)$ varies widely, the analyst will have to examine the complete time history of the thermal stress for the purpose of selecting several pertinent baseline distributions as the basis for buckling analysis. The correlation in figure 10 is enhanced by the fact that the thermal stress distribution at time = 30 sec closely resembles the thermal stress distribution at time = 20.5 sec.

Another factor complicating the problem is pertinent in this case. It is not uncommon for local thermal stresses to exceed plastic limits because thermal stress distributions can reach excessive values in local areas. This is true in this case, and the regions of plasticity can be seen in figures 11 and 12 for the times 20.5 and 30.0 sec, respectively. Most of the plasticity occurs in the curved portion of the leading-edge specimen and this part is not being analyzed as part of the plate buckling mechanism. However, the results obtained from the thermal stress (that is, the edge loads) model must be altered to account for this phenomenon. The ideal approach to this problem is a plastic analysis to acquire the precise thermal stress distribution. Expense and time factors will probably prohibit a plastic analysis if a major component is to be designed using existing finite element computer codes. An alternate approach, which is also conservative in nature, is simply to use a plasticity reduction factor so that

$$\sigma_T = \eta \sigma_{T_i} \tag{12}$$

where σ_T is the thermal stess, η is a numerical coefficient computed as the ratio of yield stress to thermal stress, and σ_{T_i} is the thermal stress at the ith element. The application involves using the stress distribution defined by the points A-B-C in figure 12. Since part of this segment extends into the curved portion of the specimen, then the distribution defined by A′-B-C is used for the flat part of the specimen corresponding to the plate buckling model. Therefore, the baseline thermal stress distribution modified for plasticity can be seen in figure 13. The distribution $\sigma(t, \eta)$ corresponds to the distribution defined by A′-B-C in figure 12. The eigenvalues were recomputed with the buckling model for the modified thermal stress distribution. The results for both sets of eigenvalues are presented in table 1. It can be seen that this modification of the load distribution had little effect on the magnitude of the eigenvalues. This is most likely owing to the fact that the modification to the distribution was close to a restrained edge.

An important assumption that has not been discussed concerns the fact that the edge loads are not the same on the two ends of the plate area selected for analysis. If the axial normal thermal stress distribution of figure 7 is examined again, it can be seen that the maximum stress occurs at the right edge of the quarter stress model. It is presumed that the stress on the left edge of the buckling model is the same. However, in reality, the stress is perhaps 40,000 lb/in.^{2} less elastically. When plasticity is considered, this differential becomes less important and may be negligible. It will be seen that this situation is even more evident when mode B is examined in the next section.

Mode B Analysis

The buckling failure which manifested itself as mode B (fig. 4) was caused by lateral normal thermal stresses (fig. 7), and the dominant buckling factor was the single free edge. A summary of the situation is presented

in figure 14 where the buckling region is shown along with lateral normal thermal stress contours. It can be seen that the large compressive lateral normal thermal stresses are concentrated in the lower left corner of the specimen. It can also be seen that the thermal stress gradients $\partial\sigma_T/\partial x$ and $\partial\sigma_T/\partial y$ are quite large. This makes the definition of a problem to be analyzed very difficult. This can be illustrated by examining the three areas of figure 14 and the corresponding edge stress conditions. The stress in the y-direction is not constant, and the edge stress on the y-faces of the plates is unequal. It can easily be seen that a variety of problems can be selected for analysis.

Area 2 was selected for NASTRAN buckling analysis. The dimensions of this area are 5/8 in. in the x-direction and 1 in. in the y-direction. The stress distribution selected varied linearly from 100,000 lb/in.^{2} at the left corners to 75,000 lb/in.^{2} at the right corners. This problem is shown in figure 15. The NASTRAN buckling model was developed from a lattice of plate elements with five plates in the x-direction and eight plates in the y-direction. The buckling analysis is summarized in figure 15. Eigenvalues for the first two modes for two boundary conditions are used to develop buckling stress distributions from the baseline thermal stress distribution (depicted by the line in fig. 15). This analysis is based on the stress distribution at time = 30.0 sec. The results of figure 15 are consistent with the fact that the specimen has buckled at time = 30.0 sec. Both mode 1 eigenvalues indicate buckling should have occurred before the baseline thermal stress distribution reached the distribution represented by the line. The mode shapes associated with the buckling analyses are presented in figure 16. The actual eigenvalues are summarized in table 2.

The mode B problem is basically an unstable situation since the plate geometry and the edge loading are greatly interdependent. Each time a different area is chosen for analysis, a different loading and a different loading gradient must be accommodated. Fortunately, in practice, the free edge, which allows the buckling strength to be critical, would either be stiffened or the end would be closed out. This would make mode A dominant over mode B and relieve the designer of some critical decisions.

CONCLUDING REMARKS

High-temperature thin-shell leading-edge buckling test data were analyzed to evaluate NASTRAN as a finite element tool for predicting thermal buckling characteristics. It was found that buckling points could be predicted quite well with NASTRAN. It was also found that the first three eigenvalues for four different sets of boundary conditions were closely packed for the primary buckling mode. As a result, the boundary conditions had much less effect on the buckling point than was anticipated. The most pronounced problem was relating the plate area to the edge stress distribution and the stress gradient. This problem requires pertinent judgment by the analyst.

Local plasticity occurred on the specimen analyzed. Plasticity tended to simplify the basic problem since it effectively equalized the stress gradient from loaded edge to loaded edge. It was concluded that the baseline edge loading (the initial loading) will be difficult to identify because of the transient nature of thermal stress. Severeal initial loadings will be required for complicated thermal stress time histories before a pertinent finite element buckling analysis will be effected. The basic mode shapes observed during the tests were correctly identified using the NASTRAN program.

Ames Research Center
Dryden Flight Research Facility
National Aeronautics and Space Administration
Edwards, California, September 23, 1987

REFERENCES

Gerard, George; and Becker, Herbert: Handbook of Structural Stability, Part I–Buckling of Flat Plates. NACA TN-3781, 1957.

Jenkins, J.M.; and Sefic, W.J.: Experimental Investigation of Thermal-Buckling Characteristics of Flanged, Thin-Shell Leading Edges. NASA TN-D-3243, 1966.

NASA-COSMIC: NASTRAN User's Manual. NASA SP-222(06), 1983.

Syracuse University: Aerospace Structural Metals Handbook. Volume 2, Nonferrous Alloys. Syracuse University Press, Dec. 1982.

Timoshenko, S.P.; and Gere, J.M.: Theory of Elastic Stability. Second Edition, McGraw-Hill Book Company, Inc., 1961.

TABLE 1.—SUMMARY OF EIGENVALUES

Edge boundary conditions[a]			Baseline eigenvalues			Eigenvalues with plasticity effect		
Ends	Top	Bottom	Mode 1	Mode 2	Mode 3	Mode 1	Mode 2	Mode 3
SS	SS	C	0.925	1.064	1.211	0.895	0.962	1.081
C	SS	C	0.860	0.894	1.100	0.915	0.946	1.197
SS	C	C	0.877	1.022	1.055	0.945	0.974	1.203
C	C	C	0.869	1.099	1.114	0.878	1.023	1.181

[a]SS—Simply supported; C—Clamped.

TABLE 2.—SUMMARY OF MODE B EIGENVALUES

Edge boundary conditions[a]				Eigenvalues	
Top	Bottom	Left edge	Right edge	Mode 1	Mode 2
C	C	F	SS	0.913	1.198
SS	C	F	SS	0.874	1.108

[a]SS—Simply supported; C—Clamped; F—Free.

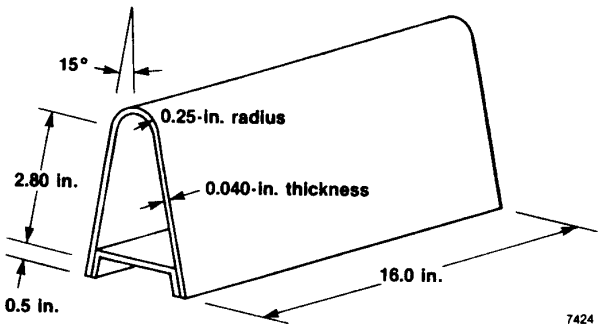

(a) Specimen geometry.

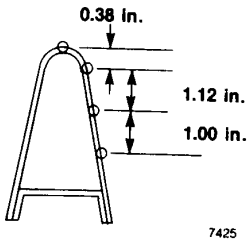

(b) Thermocouple location.

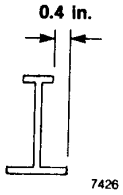

(c) 4I7.7 restraining beam.

Figure 1. Sketches showing leading-edge-specimen geometry, thermocouple location, and restraining beam.

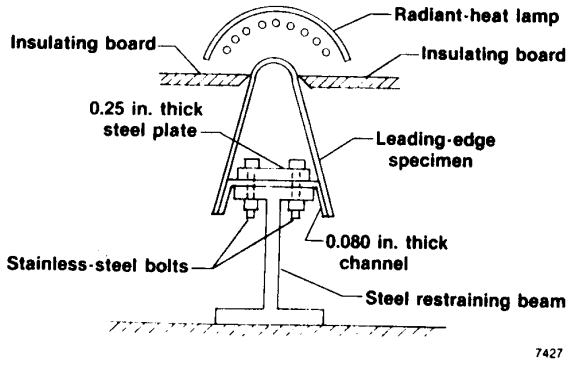

Figure 2. Sketch of test condition.

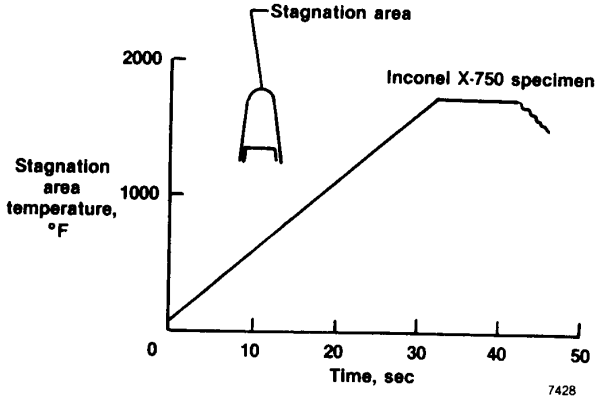

Figure 3. Programmed temperature-time histories for specimen stagnation area.

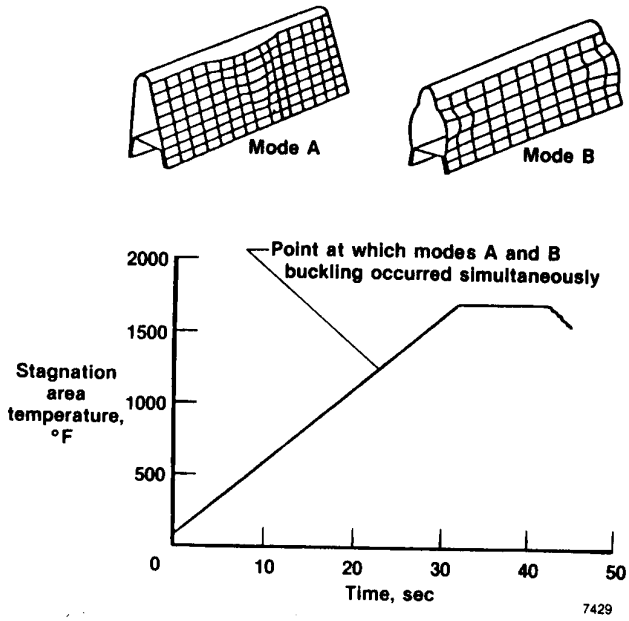

Figure 4. Mode shapes at buckling failure.

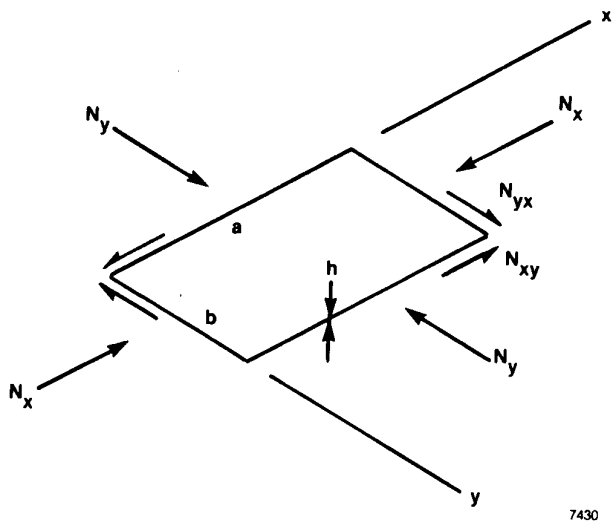

Figure 5. Plate geometry and nomenclature.

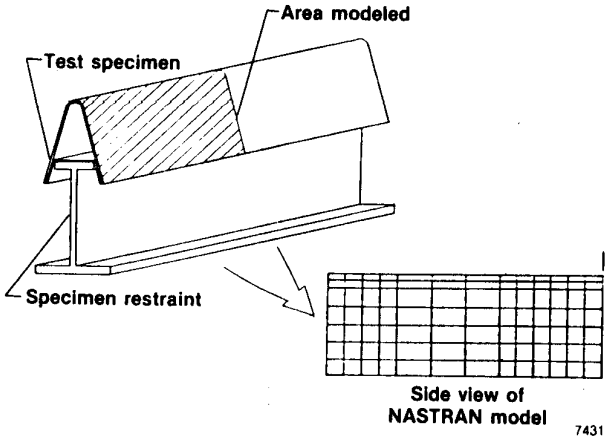

(a) Symmetrical quarter model.

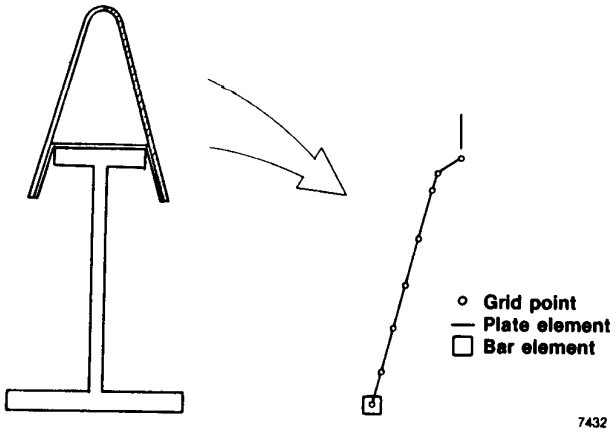

(b) End view of NASTRAN model.

Figure 6. NASTRAN stress model.

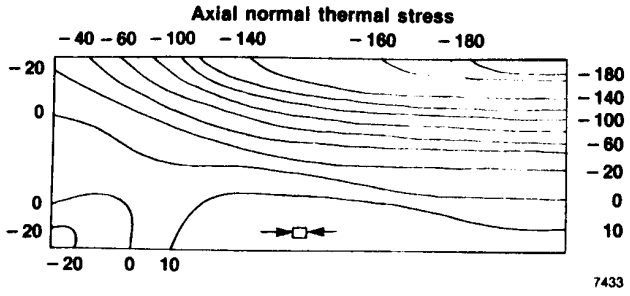

(a) Axial normal thermal stress, klb/in.^{2}.

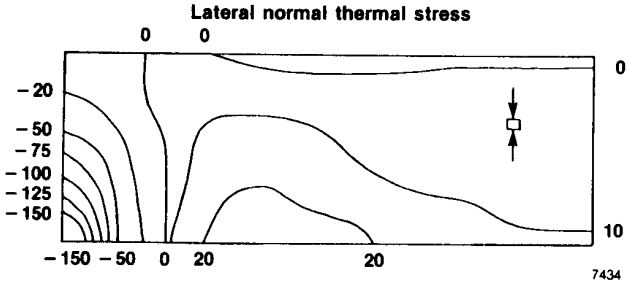

(b) Lateral normal thermal stress, klb/in.^{2}.

Figure 7. Contour map of lines of constant axial and lateral thermal stress.

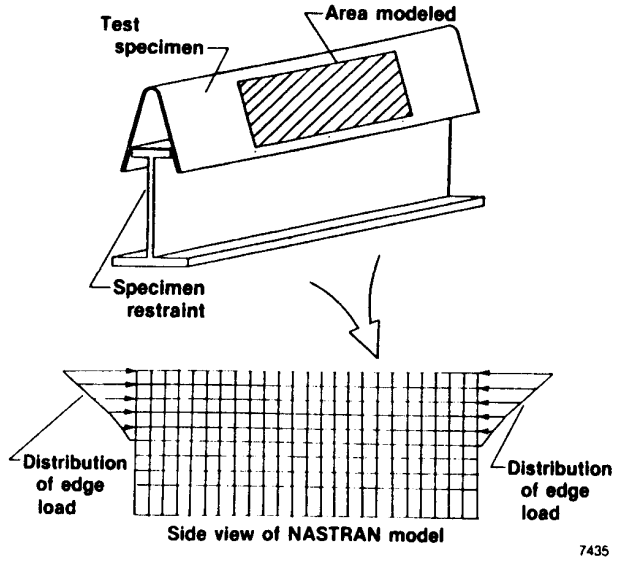

Figure 8. NASTRAN model used for buckling analysis.

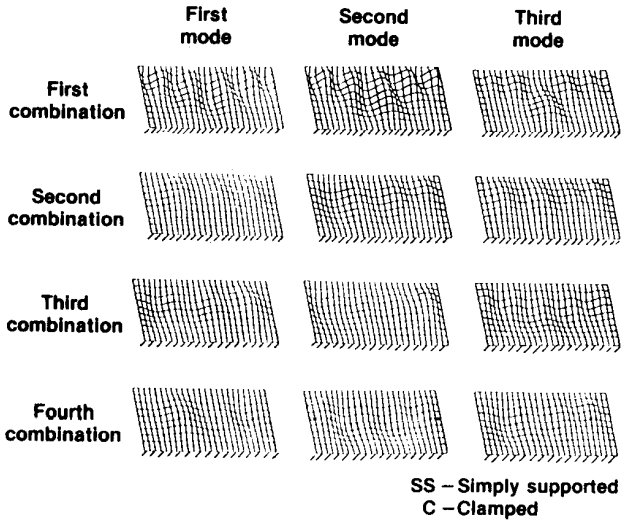

Combinations	Edge boundary conditions: Ends	Top	Bottom	Mode	Eigenvalues: 1	2	3
First	SS	SS	C		.925	1.064	1.211
Second	C	SS	C		.860	.894	1.100
Third	SS	C	C		.877	1.022	1.055
Fourth	C	C	C		.869	1.099	1.114

7436

Figure 9. First three mode shapes and eigenvalues from NASTRAN buckling analysis for various edge boundary conditions.

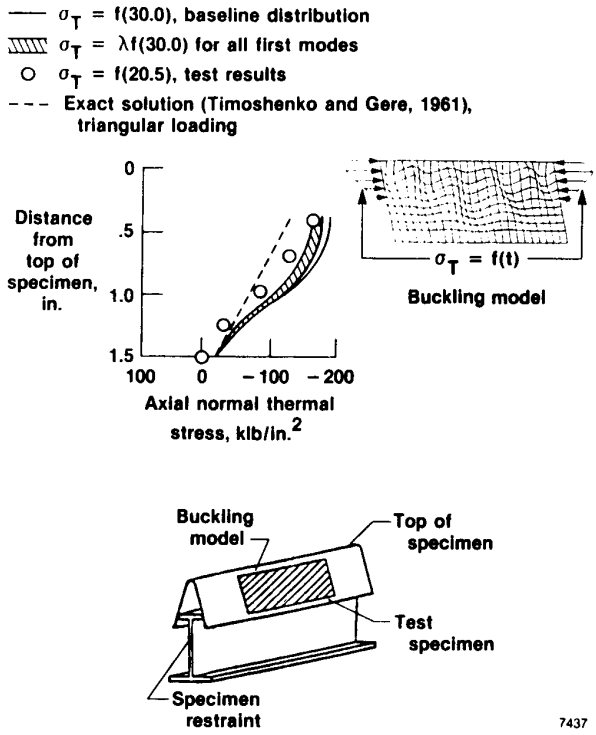

Figure 10. A comparison of NASTRAN calculated and experimentally derived thermal stress distributions at buckling.

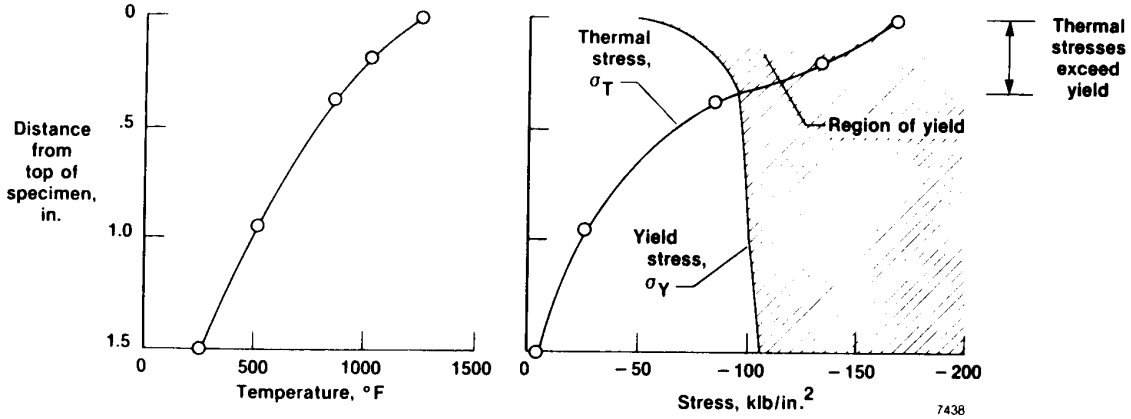

Figure 11. Illustration of region of plasticity at time = 20.5 sec.

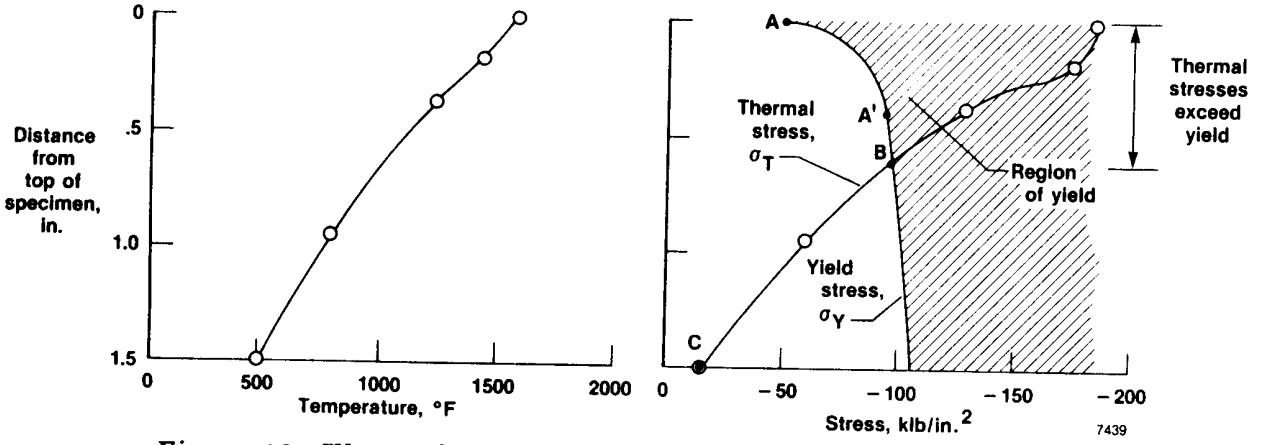

Figure 12. Illustration of region of plasticity at time = 30.0 sec.

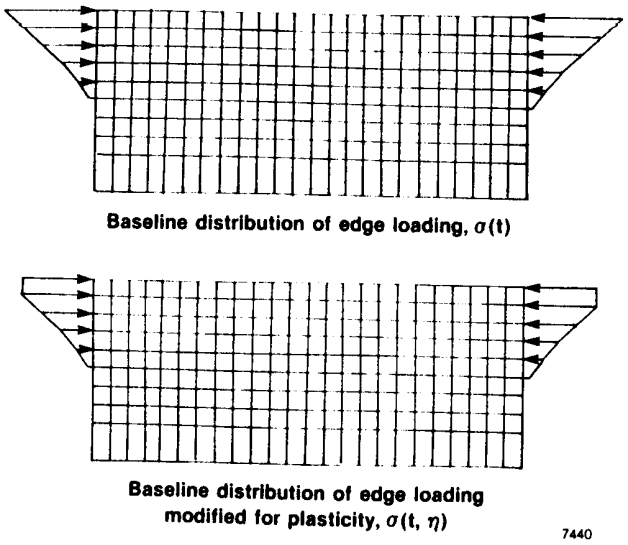

Figure 13. Baseline edge loading modified for plasticity.

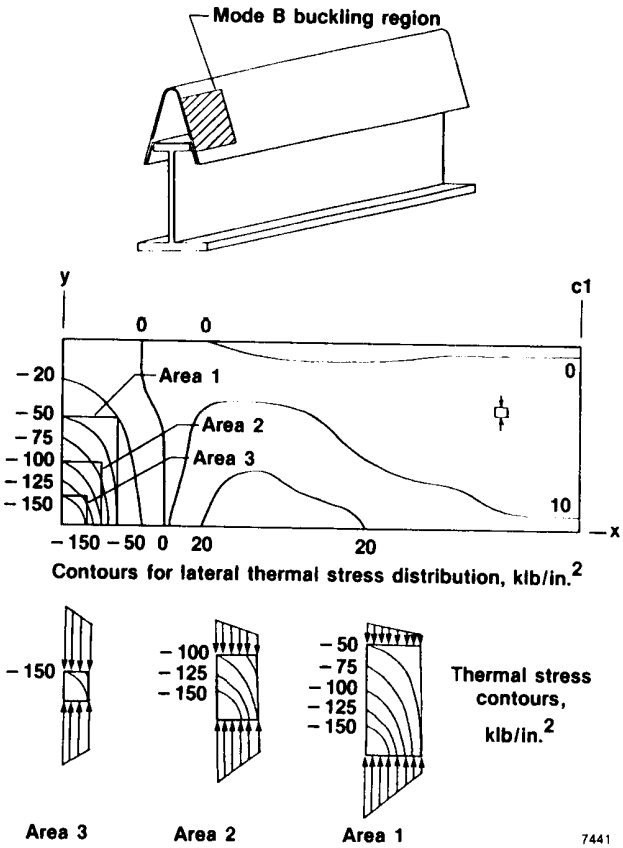

Figure 14. Examples of unstable-indeterminate problems in the mode B buckling region.

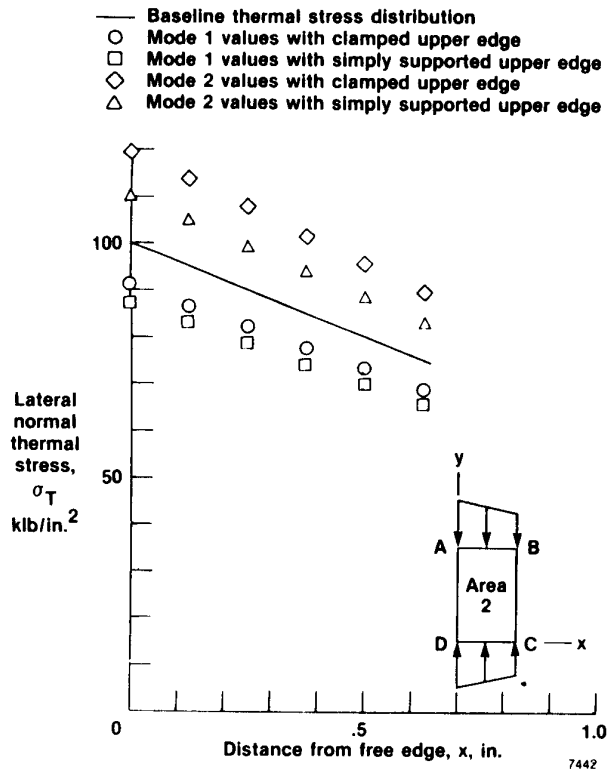

Figure 15. A comparison of NASTRAN calculated thermal stress distributions for various boundary conditions and mode shapes.

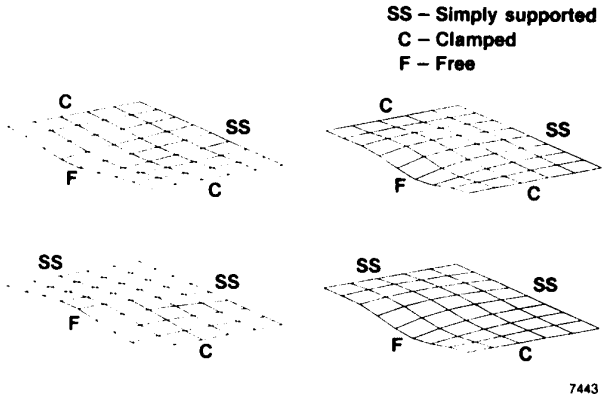

Figure 16. First two mode shapes from NASTRAN buckling analysis for various edge boundary conditions.

NASA
National Aeronautics and Space Administration

Report Documentation Page

1. Report No.	2. Government Accession No.	3. Recipient's Catalog No.
NASA TM-100416		

4. Title and Subtitle	5. Report Date
A Comparison of Experimental and Calculated Thin-Shell Leading-Edge Buckling Due to Thermal Stresses	July 1988
	6. Performing Organization Code

7. Author(s)	8. Performing Organization Report No.
Jerald M. Jenkins	H-1440
	10. Work Unit No.
	RTOP 506-43-81

9. Performing Organization Name and Address	11. Contract or Grant No.
NASA Ames Research Center Dryden Flight Research Facility P.O. Box 273, Edwards, CA 93523-5000	
	13. Type of Report and Period Covered
12. Sponsoring Agency Name and Address	Technical Memorandum
National Aeronautics and Space Administration Washington, DC 20546	14. Sponsoring Agency Code

15. Supplementary Notes

16. Abstract

High-temperature thin-shell leading-edge buckling test data are analyzed using NASA structural analysis (NASTRAN) as a finite element tool for predicting thermal buckling characteristics. Buckling points are predicted for several combinations of edge boundary conditions. The problem of relating the appropriate plate area to the edge stress distribution and the stress gradient is addressed in terms of analysis assumptions. Local plasticity was found to occur on the specimen analyzed, and this tended to simplify the basic problem since it effectively equalized the stress gradient from loaded edge to loaded edge. The initial loading was found to be difficult to select for the buckling analysis because of the transient nature of thermal stress. Multiple initial model loadings are likely required for complicated thermal stress time histories before a pertinent finite element buckling analysis can be achieved. The basic mode shapes determined from experimentation were correctly identified from computations.

17. Key Words (Suggested by Author(s))	18. Distribution Statement
Thermal stress Thermal buckling Buckling	Unclassified — Unlimited Subject category 39

19. Security Classif. (of this report)	20. Security Classif. (of this page)	21. No. of pages	22. Price
Unclassified	Unclassified	15	A02

NASA FORM 1626 OCT 86

**For sale by the National Technical Information Service, Springfield, VA 22161-2171.*